Penerbit Akademia Baru

Journal of Advanced Research in Experimental Fluid Mechanics and Heat Transfer

Journal homepage: http://www.akademiabaru.com/submit/index.php/arefmht

ISSN: 2756-8202

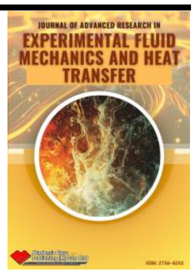

Energy Harvesting from Flow-Induced Vibrations using Piezoelectric Systems

Hafizal Yahaya[1], Mohamed Sukri Mat Ali[1,*], Alisya Sofea Norisham[1], Sharviin Subramaniam[1], Nurshafinaz Maruai[1], Ahmad Adzlan Khairi[2], Fauzan Ahmad[3]

[1] Department of Mechanical Precision Engineering, Malaysia-Japan International Institute of Technology, Universiti Teknologi Malaysia, 54100 Kuala Lumpur, Malaysia

[2] Department of Mechanical and Manufacturing Engineering, Faculty of Engineering, Universiti Malaysia Sarawak, 94300 Kota Samarahan, Sarawak, Malaysia

[3] Department of Electronic System Engineering, Malaysia-Japan International Institute of Technology, Universiti Teknologi Malaysia, 54100 Kuala Lumpur, Malaysia

ARTICLE INFO

Article history:
Received 19 March 2025
Received in revised form 9 April 2025
Accepted 9 May 2025
Available online 30 June 2025

Keywords:
Flow-induced vibration; energy harvesting; piezoelectric systems; reduced velocity; galloping

ABSTRACT

The growing demand for sustainable energy solutions has spurred interest in harnessing energy from flow-induced vibrations (FIV), a phenomenon traditionally associated with structural fatigue but now recognized for its potential in renewable energy generation. Despite advancements in piezoelectric energy harvesting, the interplay between flow dynamics, vibration characteristics and energy conversion efficiency remain inadequately understood, particularly across varying flow regimes. This study aims to experimentally investigate the relationship between FIV and piezoelectric energy harvesting, focusing on optimizing geometric configurations and flow parameters to maximize energy output. A square cylinder subjected to controlled wind tunnel flow was analysed to evaluate its dynamic response and energy conversion efficiency at different reduced velocities (U_r). The experimental methodology included free vibration testing, wind tunnel experiments and piezoelectric voltage measurements to characterize vibration amplitudes and harvested energy. Results identified three distinct regimes: vortex-induced vibration (VIV) at $U_r < 30$, transition at $30 \leq U_r \leq 40$ and galloping at $U_r > 40$. The VIV regime exhibited dominant frequency harmonics ($f = nf_0$) with moderate energy output, while the transition regime showed nonlinear energy responses due to shifting frequency components. The galloping regime demonstrated the highest energy harvesting potential, driven by sustained, large-amplitude oscillations. These findings underscore the critical role of flow-structure interactions in energy harvesting performance and provide practical insights for optimizing transducer design to enhance efficiency. This research contributes to the development of robust renewable energy systems leveraging FIV mechanisms.

* *Corresponding author.*
E-mail address: sukri.kl@utm.my (Mohamed Sukri Mat Ali)

https://doi.org/10.37934/arefmht.20.1.136149

1. Introduction

The growing need for sustainable energy sources has led to an increasing focus on energy harvesting from flow-induced vibrations (FIV). Initially considered a cause of structural fatigue, FIV is now viewed as a viable mechanism for renewable energy generation, particularly through piezoelectric transduction [1-5]. Piezoelectric energy harvesting from FIV offers a promising means of generating power in wind and water environments, making it suitable for self-powered devices and remote sensing applications [6-8].

Various studies have investigated different configurations of FIV-based energy harvesters. Shahid *et al.*, [1] examined the influence of confinement on piezoelectric energy harvesting efficiency, demonstrating that boundary conditions significantly affect power output. Islam *et al.,* [2] conducted an experimental and numerical study on an elastically mounted circular cylinder, showing that the highest power generation occurs within the lock-in region where resonance conditions amplify vibrations. Masoumi *et al.,* [3] explored a hybrid piezoelectric-electromagnetic harvester and found that combining multiple energy conversion mechanisms enhances the energy harvesting range and efficiency.

The growing need for sustainable energy sources has led to an increasing focus on energy harvesting from flow-induced vibrations (FIV) [4]. Initially considered a cause of structural fatigue, FIV is now viewed as a viable mechanism for renewable energy generation, particularly through piezoelectric transduction [1-5] Piezoelectric energy harvesting from FIV offers a promising means of generating power in wind and water environments, making it suitable for self-powered devices and remote sensing applications [7-9].

Recent advancements have also highlighted the impact of vortex dynamics on energy conversion efficiency. Rashki *et al.,* [5] analysed the effects of marine growth on the performance of two-degree of-freedom (2DoF) VIV-based piezoelectric energy harvesters and found that biofouling significantly reduces energy extraction efficiency. Zhang *et al.,* [6] introduced passive control techniques to enhance the energy harvested from vortex-induced oscillations. Similarly, Özkan *et al.,* [7] studied piezoelectric energy harvesting from flag fluttering at low wind speeds, demonstrating that fabric material selection and aspect ratio play crucial roles in maximizing output voltage.

The effectiveness of FIV-based energy harvesting is strongly governed by several dimensionless parameters, including the reduced velocity (Ur), Scruton number (Sc) and Strouhal number (St). The reduced velocity is given by Eq. (1):

$$U_r = \frac{U}{f_n D} \tag{1}$$

where U is the free-stream velocity, f_n is the natural frequency and D is the characteristic length of the bluff body. The lock-in region, where vortex shedding frequency matches the natural frequency of the structure, leads to amplified oscillations and enhanced power generation [8,10].

The Scruton number, which quantifies the damping effect on vibration, is defined as:

$$Sc = \frac{2m\zeta}{\rho D^2} \tag{2}$$

where m is the mass per unit length, ζ is the damping ratio and ρ is the fluid density. Higher Sc values reduce oscillation amplitudes, while lower values facilitate greater energy extraction. The Strouhal number, which characterizes vortex shedding frequency, is expressed as:

$$St = \frac{f_s D}{U} \tag{3}$$

where f_s is the shedding frequency. When St aligns with the natural frequency of the structure, resonance conditions optimize energy harvesting [8,9].

Despite extensive research on FIV-based energy harvesting, critical gaps persist in understanding the nonlinear interplay between flow regimes, vibration dynamics and piezoelectric energy conversion efficiency. While theoretical and computational studies provide insight into these interactions, experimental validation across varying flow conditions is needed [10,11]. Previous studies have primarily focused on isolated regimes (e.g., VIV or galloping) or idealized conditions, neglecting the transitional behaviours that dictate real-world performance. For instance, the impact of reduced velocity (U_r) on harmonic energy distribution in piezoelectric systems remains underexplored, particularly during the shift from VIV to galloping. Additionally, while theoretical models predict optimal energy harvesting conditions, experimental validations across a broad U_r range—especially for non-circular bluff bodies like square cylinders—are scarce. Addressing these gaps is essential to optimize transducer designs for adaptive energy harvesting in variable flow environments (e.g., urban wind corridors or underwater currents). This study aims to experimentally investigate the relationship between FIV and piezoelectric energy harvesting, focusing on optimizing geometric configurations and flow parameters for maximum energy output. This study bridges these gaps by systematically characterizing the energy harvesting potential across all three regimes (VIV, transition and galloping), offering empirical insights into frequency response, amplitude thresholds and nonlinear strain coupling in piezoelectric systems.

2. Methodology

2.1 Problem Geometry

The problem under investigation is a square cylinder immersed in a uniform flow of U_∞. Similar to any blunt body shape, flow over a square cylinder produces Karman vortices due to flow separations. The forming of a Karman vortex street generates instantaneous aerodynamic fluctuations on the body. In this study, the square cylinder is supported by a spring-damping system, as visualized in Figure 1, so that vibration of the cylinder is controlled following the stiffness and damping values of the system. This study focusses to explore the relation between velocity of the incoming flow with the harvested energy from vibration of the cylinder. The mass-spring-damping criteria is kept constant and the chosen values are based on the previously available similar studies (on flow induced vibration but not the same for the utilizing piezoelectric) [12-15].

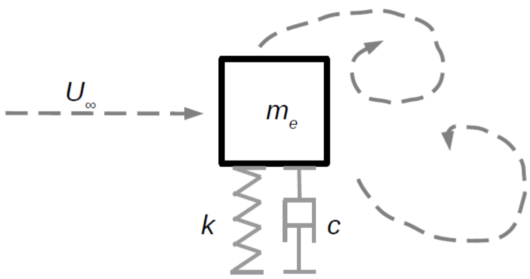

Fig. 1. Problem geometry under investigation

Table 1 lists and compares the mass-spring damping values for the current study and also previous similar studies. While the effective mass for the current study is the same as previous studies (except for Kawabata *et al.,* [12]), other parameters having higher magnitude compare to previous studies. This is mainly due to high spring (k) constant and high damping factor ζ.

Table 1
Compares the mass-spring damping values

Parameter	Kawabata *et al.,* [12]	Ismail *et al.,* [13]	Maruai *et al.,* [15]	Methal *et al.,* [14]	current
Effective Mass, me $[kg]$	0.110	0.145	0.145	0.145	0.145
Spring Constant, k $[N/m]$	1181	1173	1173	1422	1535
Natural Frequency, fn $[Hz]$	16.5	14.2	14.2	15.9	16.49
Logarithmic damping factor, δ	0.0270	0.0275	0.0275	0.0427	0.0505
Damping ratio, ζ	0.0043	0.0047	0.0044	0.0068	0.0080
Scruton number, $Sc\,\frac{2m\zeta}{\rho D^2}$	24.1	32.2	31.2	45.6	51.1

2.2 Wind Tunnel Facility

The experiments were conducted in a subsonic open-circuit wind tunnel at a controlled wind engineering laboratory. The test section dimensions are $0.8 \times 0.46 \times 0.38$ m, ensuring a low solid blockage ratio $\left(\frac{A_b}{A_w} < 40\%\right)$. The flow speed was varied between 2 m/s to 30 m/s ($3\times10^4 \lesssim Re \lesssim 5$ 10^5) to analyse its impact on vibration and energy harvesting. Figure 2 shows the test section of the wind tunnel.

Fig. 2. Subsonic open wind tunnel

The test section is specifically designed for flow induced vibration investigations. Similar design has been opted by Kawabata *et al.,* [12], Methal *et al.,* [14] and Mohamed *et al.,* [16]. The test section is equipped with twin plate springs on both side of the test section. The dimensions of the spring plate are 0.5 m in length, 4.0 mm in width, 1.0 mm in thickness and it is made from spring steel material. The spring stiffness can be adjustable by adjusting the spring length. For this recent study, the spring stiffness is made constant at $k = 1535\ \mathrm{Nm}^{-1}$.

2.3 Measurement Instruments

The parameters of interest in this study are vibration amplitude $(y(t))$ and the magnitude of energy $(V(t))$ being generated from the vibration. To measure these parameters, laser displacement sensor and piezoelectric film transducer have been used.

Omron ZX-LDA11 laser displacement sensors were installed on the both side of the wind tunnel test section. This enable transverse movement being measured at both end of the cylinder. Figure 3 shows the setup of laser displacement sensor at one side of the wind tunnel section. The signal from sensors were amplified using Omron ZX-LD100 amplifier before it being connected to oscilloscope.

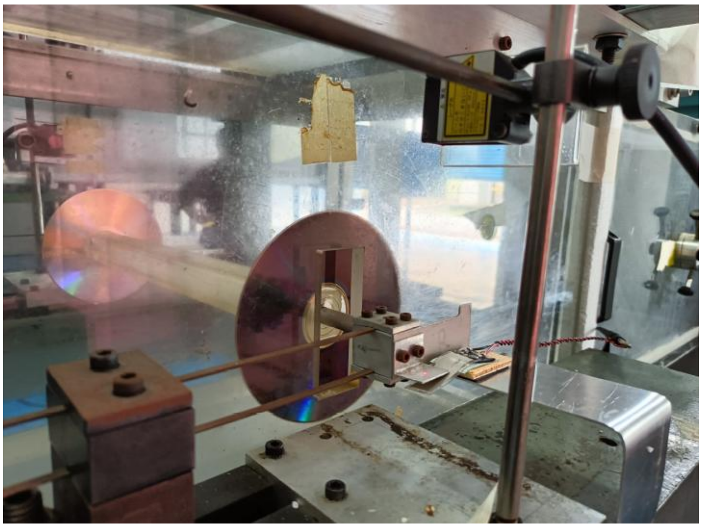

Fig. 3. Laser displacement sensor

LDTO-028K PVDF piezoelectric film vibration has been used as the transducer to convert the vibration into voltage. It has sensitivity of 50 mV/g. The piezoelectric is placed at the end of cylinder as shown in Figure 4(a) and the distance beyond its clamp is 10 mm. See Figure 4(b) for the close-up view of the piezoelectric. The piezoelectric was directly connected to an oscilloscope recorded voltage output. The free stream velocity inside the test section was measured using pitot static. The pressure different was digitally calculated using DPC-202N micro manometer. It is a pressure gauge in Figure 5 equipped with two pressure ports (HI and LOW) which measure and indicate pressure differences up to 2000 Pa.

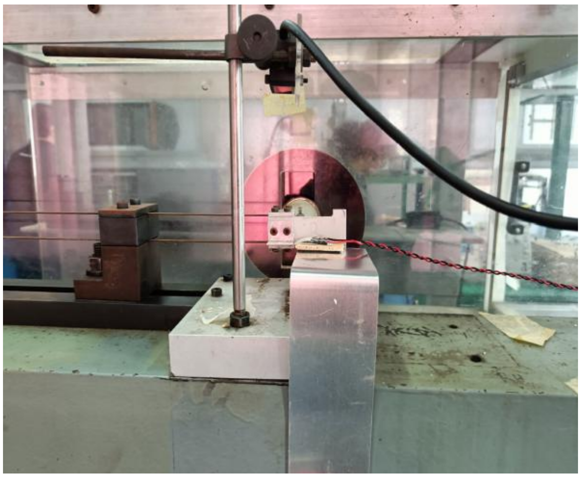

(a)

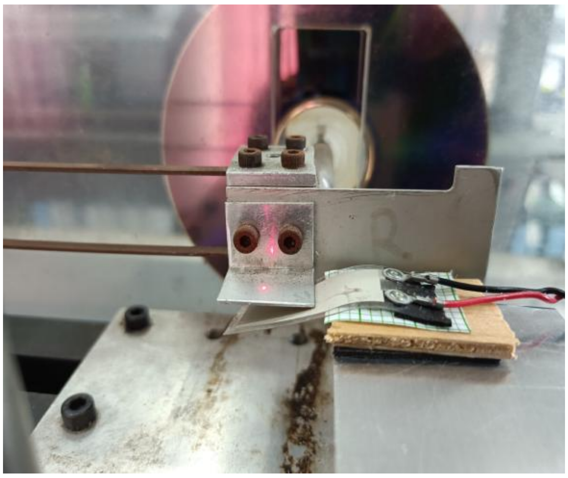

(b)

Fig. 4. Piezoelectric (a) Piezoelectric installed on the side of wind tunnel (b) Close up view of the piezoelectric

Fig. 5. Pressure gauge for pitot static tube

3. Results

3.1 Free Vibration Testing

Free vibration testing is a fundamental approach for characterizing the dynamic properties of a mechanical system. In the context of energy harvesting from flow-induced vibrations, such testing is essential to determine key parameters, including natural frequency, damping ratio and stiffness, which influence the energy harvesting performance. In a free vibration test, a system is initially displaced from its equilibrium position and then allowed to oscillate freely under the influence of its inherent restoring forces. For a simple linear mass-spring-damper system, the governing equation of motion is given by:

$$m\ddot{y}(t) + c\dot{y}(t) + ky(t) = 0 \tag{4}$$

where m is the mass of the system, c is the damping coefficient, k is the stiffness of the spring and $y(t)$ is the transverse displacement as a function of time. The solution to this equation depends on the damping ratio, defined as:

$$\zeta = \frac{c}{2\sqrt{mk}} \tag{5}$$

If $\zeta < 1$ (underdamped case), the system undergoes oscillatory motion and the displacement can be expressed as:

$$y(t) + Y_0 e^{-\zeta\omega_n t} cos(\omega_d t + \emptyset) \tag{6}$$

where Y_0 is the initial amplitude, $\omega_n = \sqrt{\frac{k}{m}}$ is the natural frequency of the system, $\omega_d = \omega_n\sqrt{1-\zeta^2}$ is the damped natural frequency and $\emptyset$ is the phase angle.

The experimental setup involves displacing the square cylinder and recording the response using laser displacement sensors. The time-history data of displacement is then analysed to extract key parameters. The natural frequency f_n is calculated from the time period of oscillations:

$$f_n = \frac{1}{T} \tag{7}$$

where T is the average time period between successive peaks of the displacement signal. Using Fourier Transform, the frequency domain representation of the displacement signal can also be analysed, where the dominant frequency corresponds to f_n.

The logarithmic decrement method is commonly used to estimate the damping ratio ζ. It is defined as:

$$\delta = ln\left(\frac{y_n}{y_{n+1}}\right) \tag{8}$$

where y_n and y_{n+1} are the amplitudes of two successive peaks. The damping ratio can then be calculated as:

$$\zeta = \frac{\delta}{\sqrt{4\pi^2+\delta^2}} \tag{9}$$

The stiffness k of the spring can be determined from the natural frequency:

$$k = m\omega_n^2 = m(2\pi f_n)^2 \tag{10}$$

Free vibration testing also provides insights into the energy distribution across frequencies, which can be visualized using Power Spectral Density (PSD) plots. The PSD of the displacement signal is calculated as:

$$PSD(f) = \frac{|\hat{Y}(f)|^2}{T} \tag{11}$$

where $\hat{Y}(f)$ is the Fourier Transform of the displacement signal and T is the duration of the signal. Peaks in the PSD correspond to the natural frequencies of the system.

Table 2

Trial (xi)	1	2	3	$\bar{y}$	σ
f_N [Hz]	16.30	16.30	16.30	16.30	0
k [N/m]	1520.91	1520.90	1520.91	1520.91	0

Three free vibration testing have been made. Figure 6(a) to 6(c) show the time histories of the fluctuating amplitude and its corresponding spectrum. A clear tonal is observed in the spectrum indicating its natural frequency of the mass-spring damping system. The same values have been obtained from the three measurements giving the standard deviation of zero.

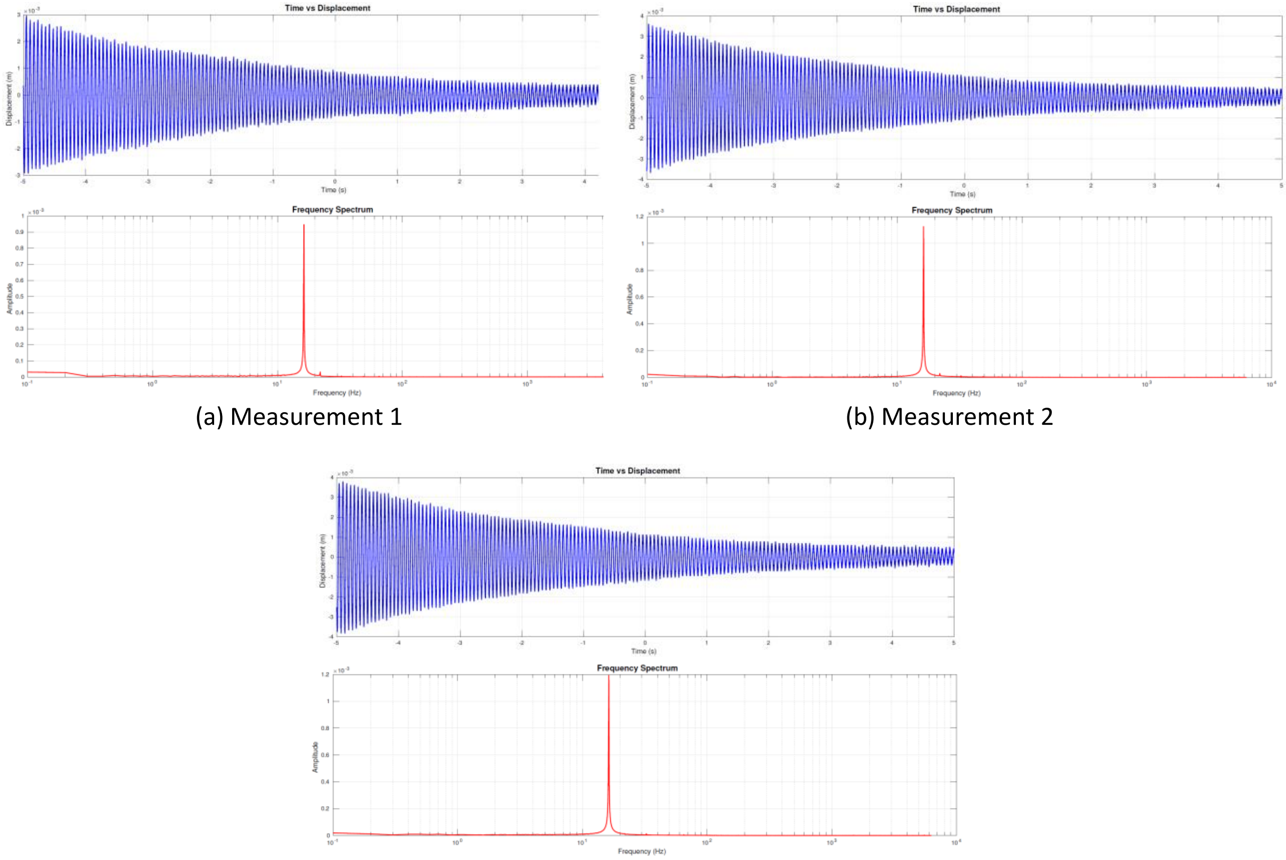

(a) Measurement 1 (b) Measurement 2

(c) Measurement 3

Fig. 6. Free vibration test

3.2 Effect of Free Stream Velocity on Vibration Amplitude

This section discusses the relationship between the dimensionless vibration amplitude y_{rms}/D and the reduced velocity (U_r) in the context of Flow-Induced Vibrations (FIV). The analysis considers theoretical aspects, including vortex-induced vibrations (VIV) and galloping. Figure 7 presents the square cylinder vibration behaviour for a wide range of reduced velocity, U_r. The x-axis, representing the reduced velocity:

$$U_r = \frac{U}{f_n D} \tag{12}$$

where U is the flow velocity, f_n is the natural frequency and D is the characteristic diameter. The y-axis shows the root-mean-square (RMS) vibration amplitude, normalized by D. At low reduced velocities $(U_r < 20)$, vibration amplitudes are small and nearly constant. As U_r increases beyond 20, small oscillations appear, suggesting the onset of vortex-induced vibrations (VIV). Around $U_r \approx 30$, a significant increase in amplitude is observed, followed by fluctuations, likely due to mode transitions. For higher reduced velocities $(U_r > 40)$, the amplitude increases steadily, indicating the onset of galloping.

FIV occurs due to the interaction between fluid forces and a structure, leading to oscillations. The key mechanisms are vortex-induced vibration (VIV) and galloping. VIV arises from periodic vortex shedding from a bluff body. It typically occurs at moderate U_r values, with vibration amplitudes increasing gradually but remaining bounded due to the lock-in phenomenon. In the figure, small amplitude vibrations at moderate $U_r(\approx 20-30)$ suggest VIV initiation.

Galloping is an aerodynamic instability, common in non-circular cross-sections (e.g., rectangular, D-section or ice-covered cables). Unlike VIV, galloping leads to unbounded vibration growth as U_r increases. The steady increase in amplitude beyond $U_r \approx 40$ suggests galloping onset with nonlinear vibration amplification.

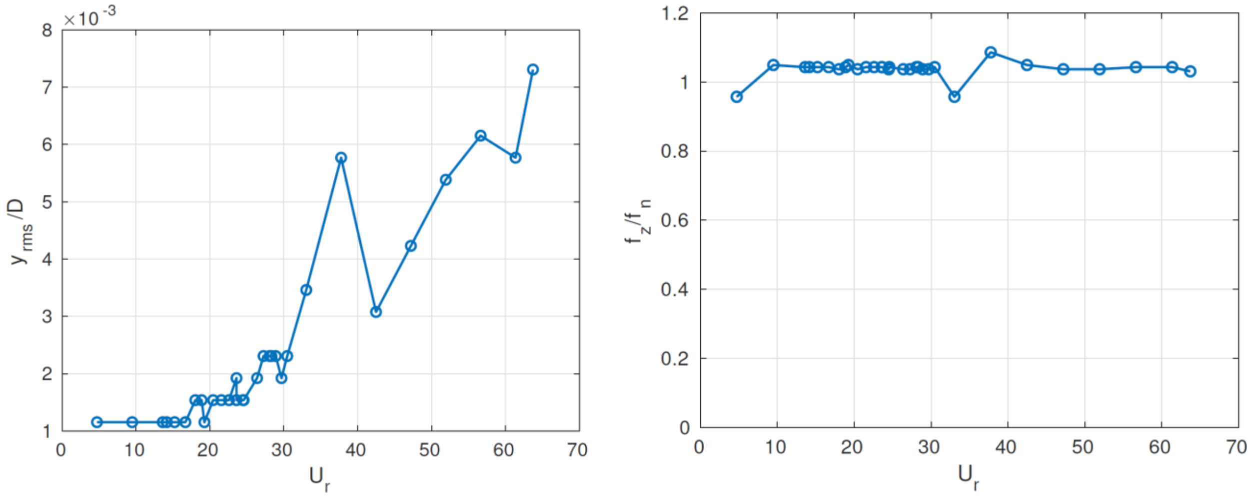

(a) Root mean square, y_{rms}, of the vibration (b) Power spectrum density (PSD) of the vibration

Fig. 7. Vibration behaviour for a wide range of reduced velocity, U_r

The plot likely captures a transition from limited-amplitude VIV to unbounded galloping at higher Ur. Excessive oscillations due to galloping can lead to structural failure. Mitigation strategies include damping solutions (e.g., tuned mass dampers) to reduce oscillations, cross-section modifications (e.g., aerodynamic fairings) to suppress galloping and predictive modelling through computational and experimental studies.

Figure 7(b) shows the variation of vibration frequency ratio (f_z/f_n) with respect to reduced velocity. The frequency ratio remains close to unity at low and moderate reduced velocities $(U_r < 30)$, indicating that the vibration is primarily governed by the natural frequency of the system, a characteristic of VIV lock-in behaviour. However, at $U_r \approx 30-40$, a shift in frequency is observed, followed by stabilization near unity again, suggesting mode transitions or changes in flow-structure interaction.

3.3 Effect of Free Stream Velocity on Harvested Energy

Figure 8 presents the behaviour of energy harvesting from flow-induced vibrations using a piezoelectric system attached to a square cylinder. Figure 8(a) shows the harvested energy in terms of voltage output, while Figure 8(b) illustrates the frequency ratio of the fluctuating energy. At low reduced velocities, the harvested energy remains small due to low vibration amplitudes. As U_r increases beyond 20, a gradual increase in energy is observed, coinciding with the onset of VIV. Around $U_r \approx 30-40$, the harvested energy experiences a sharp increase, likely due to higher vibration amplitudes and enhanced strain in the piezoelectric material. At higher U_r, particularly in the galloping regime $(U_r > 40)$, energy harvesting continues to increase significantly due to large, sustained oscillations. The frequency ratio of the fluctuating energy follows a trend similar to the vibration frequency, confirming that the harvested energy directly correlates with the vibrational behaviour of the structure.

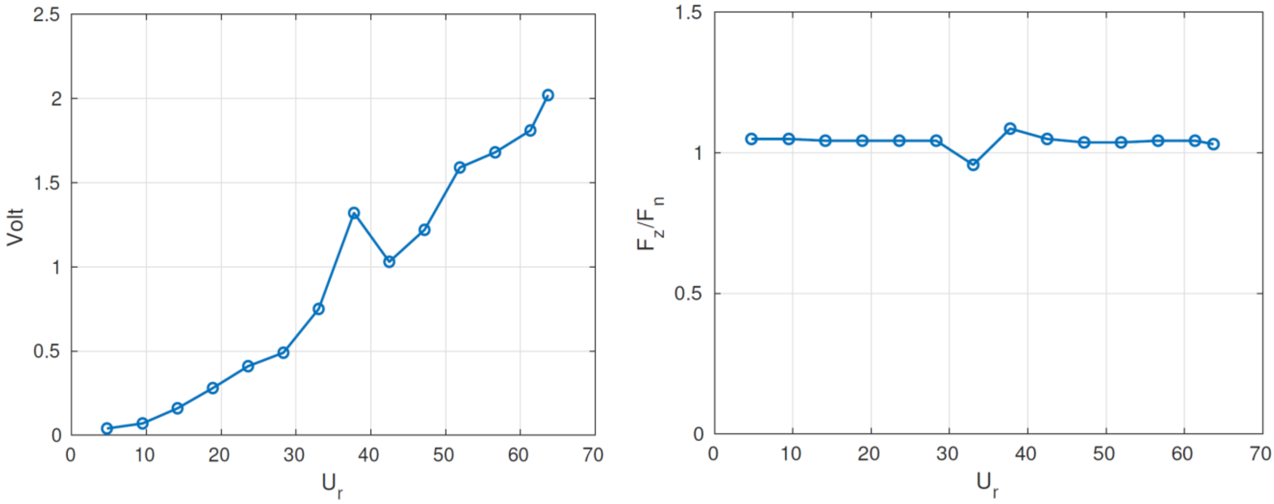

(a) Energy harvested (b) Frequency of the fluctuating energy

Fig. 8. Behaviour of the harvested energy at a wide range of reduced velocity, U_r

Piezoelectric energy harvesting relies on the direct conversion of mechanical strain into electrical energy. As the structure oscillates, strain is induced in the piezoelectric material, generating an electrical charge. The amount of energy harvested depends on the amplitude and frequency of oscillations. During VIV, energy generation remains moderate due to limited vibration amplitudes. However, in the galloping regime, the oscillations become much stronger, allowing for greater energy conversion efficiency. The nonlinearity in galloping-induced oscillations enhances the strain experienced by the piezoelectric material, making it a promising mechanism for maximizing energy output.

3.4 Vortex Induced Vibration Regime $(U_r < 30)$

In the vortex-induced vibration (VIV) regime, the signals exhibit harmonic components at frequencies $f = nf_0$, where f_0 represents the fundamental frequency of the system.

For lower reduced velocities $(U_r = 9.4)$, the power spectral density (PSD) plot shows a dominant peak at $f = f_0$, indicating the primary oscillation mode of the structure. Additionally, higher harmonics at $f = 2f_0$ and $f = 3f_0$ are present but with lower intensity.

As the reduced velocity increases to $U_r = 18.9$, the dominant frequency remains at $f = f_0$, with the second harmonic $f = 2f_0$ maintaining significant energy. However, the third harmonic $f = 3f_0$ starts to weaken, suggesting a redistribution of energy toward the lower harmonics.

At the highest reduced velocity $(U_r = 28.3)$, the fundamental frequency f_0 remains the most prominent, while the second harmonic $f = 2f_0$ is still noticeable. The third harmonic $f = 3f_0$, however, is significantly weakened compared to the lower velocity cases, indicating that as U_r increases, the energy concentration shifts primarily to the fundamental and second harmonic frequencies.

This behaviour suggests that in the VIV regime, the system predominantly oscillates at its natural frequency [17,18], while higher harmonics diminish as the reduced velocity increases, particularly at $f = 3f_0$.

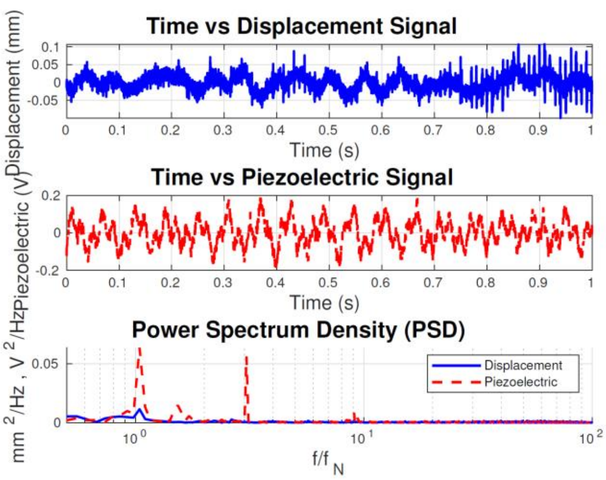

(a) $U_r = 9.4$

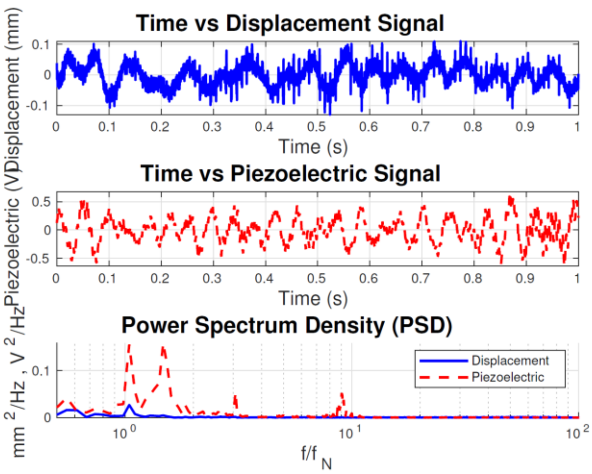

(b) $U_r = 18.9$

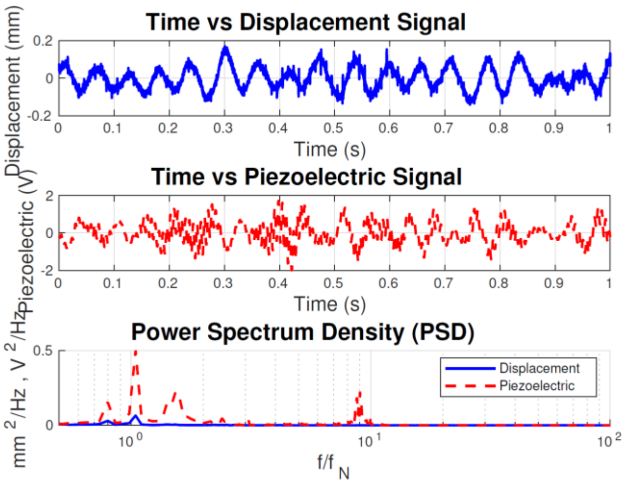

(c) $U_r = 28.3$

Fig. 9. Signals of vibration and harvested energy in vortex induced vibration regime

3.5 Transition Regime $(30 \lesssim U_r \lesssim 40)$

In the transition regime, the signals exhibit frequency components primarily at the fundamental frequency f_0, but the harmonic structure observed in the vortex-induced vibration (VIV) regime starts to weaken and change in amplitude.

For the case of $U_r = 33$, the power spectral density (PSD) plot reveals a dominant peak at $f = f_0$, similar to the VIV regime. However, the second harmonic at $f = 2f_0$ shows a reduced amplitude compared to the previous cases, indicating a transition towards a different dynamic response. The third harmonic $f = 3f_0$ is further weakened, signifying a decrease in nonlinear energy transfer.

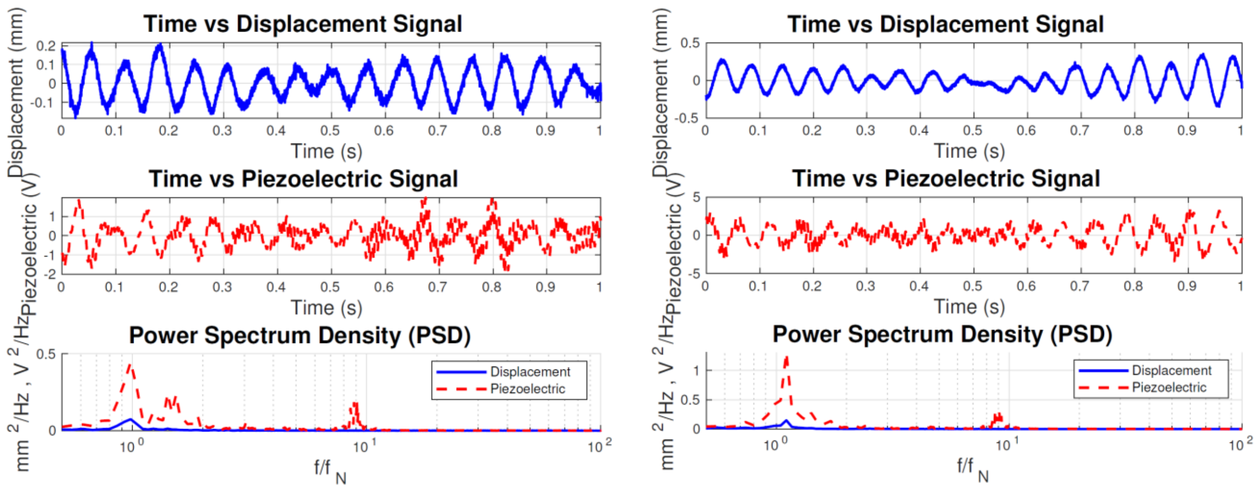

(a) $U_r = 33$ (b) $U_r = 33.8$

Fig. 10. Signals of vibration and harvested energy in transition regime

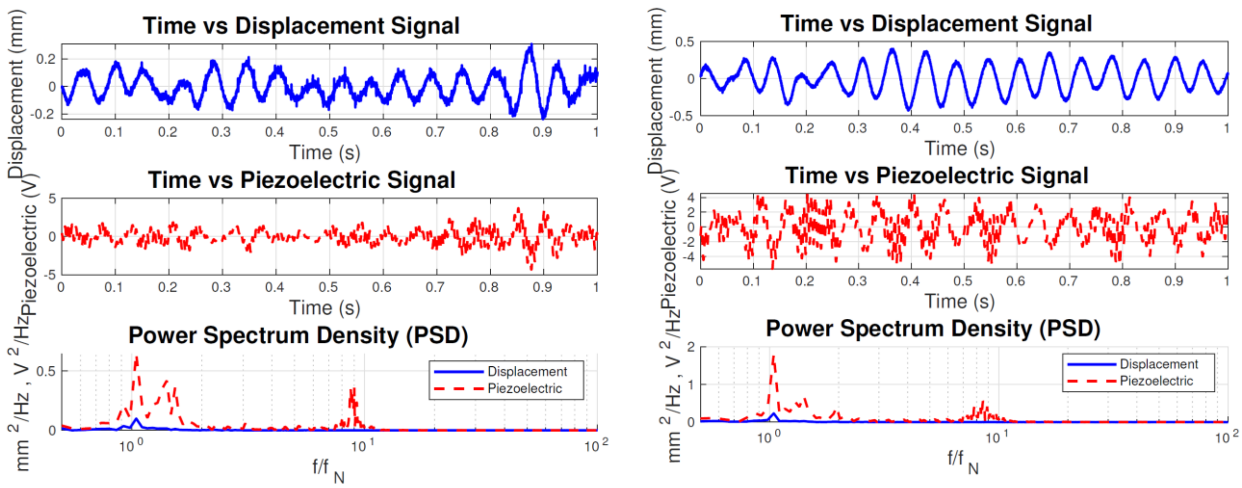

(a) $U_r = 42.5$ (b) $U_r = 63.7$

Fig. 11. Signals of vibration and harvested energy in galloping regime

At $U_r = 33.8$, the fundamental frequency f_0 remains the dominant component, but the overall vibration amplitude decreases slightly. The second harmonic at $f = 2f_0$ is still present but exhibits lower energy, while the third harmonic $f = 3f_0$ is nearly absent. This trend suggests that as U_r increases further in the transition regime, the system begins to shift away from the strong harmonic response seen in VIV.

The transition regime thus represents an intermediate state where the oscillatory behaviour shifts from a strong harmonic-dominated response to a more complex or weakened nonlinear interaction [19,20], leading to a reduction in higher harmonic amplitudes, especially at $f = 3f_0$.

3.6 Galloping Regime $(U_r > 40)$

In the galloping regime, the system exhibits a strong periodic response characterized by a dominant frequency at $f = f_0$, with higher displacement amplitudes compared to the vortex-induced vibration (VIV) and transition regimes.

For $U_r = 42.5$, the power spectral density (PSD) plot shows a distinct peak at $f = f_0$, representing the primary mode of oscillation. The second harmonic at $f = 2f_0$ is present but with a lower intensity, while the third harmonic at $f = 3f_0$ is significantly diminished. The displacement signal shows a more regular periodic behaviour and the piezoelectric signal follows the same trend with noticeable variations in amplitude.

At $U_r = 63.7$, the dominant frequency remains at $f = f_0$, but the overall amplitude of oscillation has increased. The periodic nature of the displacement signal is even more pronounced, suggesting a stable galloping motion. The PSD indicates that the energy is mostly concentrated at the fundamental frequency, with only minimal contributions from higher harmonics. The second harmonic at $f = 2f_0$ is weaker than in previous cases and the third harmonic $f = 3f_0$ is nearly absent.

The galloping regime is characterized by a sustained, high-amplitude periodic motion where the energy is largely concentrated at the fundamental frequency f_0, while higher harmonics weaken as the reduced velocity increases. This behaviour differentiates galloping from VIV, where multiple harmonics played a more significant role in the system's dynamics [21].

4. Conclusions

This study investigated the feasibility of energy harvesting from flow-induced vibrations (FIV) using a piezoelectric system. Through controlled wind tunnel experiments on a square cylinder, the research examined the influence of reduced velocity on vibration characteristics and harvested energy across different flow regimes: vortex-induced vibration (VIV), transition and galloping.

The results demonstrated that in the VIV regime $(U_r < 30)$, the system exhibited dominant frequency harmonics at $f = nf_0$, where f_0 is the fundamental frequency. The energy was primarily concentrated at the fundamental and second harmonics, while the third harmonic weakened as U_r increased. The transition regime $(30 \lesssim U_r \lesssim 40)$ marked a shift where higher harmonics gradually diminished, leading to a more complex vibrational response. Finally, in the galloping regime $(U_r > 40)$, the system displayed high-amplitude periodic oscillations dominated by the fundamental frequency, with minimal contributions from higher harmonics.

The relationship between vibration and harvested energy was evident across all regimes. As the reduced velocity increased, the harvested energy followed the trend of vibration amplitude. In the VIV regime, energy output was moderate due to the limited oscillation amplitude. The transition regime exhibited a non-linear energy response due to frequency shifts and dynamic changes in the wake-structure interaction. The galloping regime produced the highest energy output, as the sustained, large-amplitude vibrations resulted in increased strain on the piezoelectric material, leading to greater energy conversion efficiency.

These findings contribute to a deeper understanding of FIV dynamics and their impact on energy harvesting performance. The insights gained from this study can aid in optimizing structural and transducer designs for enhanced energy conversion efficiency in various fluid flow conditions.

Acknowledgement
The authors acknowledge the financial support by Universiti Teknologi Malaysia under Fundamental Research Grant, reference number PY/2023/01864 and cost centre number Q.K130000.3810.22H98.

References
[1] Shahid, H., E. Uddin, A. Abdelkefi, U. Latif, M. Shah, M. Awais and M. Zhao. "Effectiveness of energy harvesting systems subjected to flow-induced vibrations in confined spaces." *Renewable and Sustainable Energy Reviews* 210 (2025): 115183. https://doi.org/10.1016/j.rser.2024.115183

[2] Islam, Md, Ussama Ali and Shital Mone. "Harnessing flow-induced vibrations for energy harvesting: Experimental and numerical insights using piezoelectric transducer." *PLoS One* 19, no. 6 (2024): e0304489. https://doi.org/10.1371/journal.pone.0304489

[3] Masoumi, Y., F. Taheri-Behrooz and Seyyed M. Hasheminejad. "Numerical study of a synergistic hybrid energy harvesting system for bladeless wind turbines." *Energy conversion and management* 307 (2024): 118342. https://doi.org/10.1016/j.enconman.2024.118342
[4] Ahmadi, Muhammad Aiman, Mohd Maruai, Nurshafinaz, Haniff, Mohd Fadzli, Mohammad, Ahmad Faiz, Mohd Redzuan, Farah and Mohd Yusuf, Shahir. "Numerical Investigation on Tandem Body Configurations in Prospect to Enhance Low Wind Energy Harvesting." *Semarak Engineering Journal*, 3(1), (2024): 9–13.
[5] Rashki, M. R., K. Hejazi, V. Tamimi, M. Zeinoddini and H. Ashrafipour. "Impacts of hard marine growth on 2DoF VIV-based piezoelectric energy harvesting." *Renewable Energy* 231 (2024): 120913. https://doi.org/10.1016/j.renene.2024.120913
[6] Zhang, Lanbin, Bo Meng, Yun Tian, Xiangkai Meng, Xiaobo Lin, Yixiang He, Chenyang Xing, Huliang Dai and Lin Wang. "Vortex-induced vibration triboelectric nanogenerator for low speed wind energy harvesting." *Nano Energy* 95 (2022): 107029. https://doi.org/10.1016/j.nanoen.2022.107029
[7] Özkan, Musa, Onur Erkan and Sinan Basaran. "Flag Fluttering-Triggered Piezoelectric Energy Harvester at Low Wind Speed Conditions." *Energy Technology* 12, no. 4 (2024): 2301194. https://doi.org/10.1002/ente.202301194
[8] Liang, Ganggang, Daoli Zhao, Pengcheng Guo, Xin Wu, Haipeng Nan and Weipeng Sun. "Performance enhancement of hydrodynamic piezoelectric energy harvester by array disturbance." *Energy Conversion and Management* 298 (2023): 117775. https://doi.org/10.1016/j.enconman.2023.117775
[9] Kang, Jin Gu, Hyeukgyu Kim, Sangwoo Shin and Beom Seok Kim. "Fluid flow to electricity: Capturing flow-induced vibrations with micro-electromechanical-system-based piezoelectric energy harvester." *Micromachines* 15, no. 5 (2024): 581. https://doi.org/10.3390/mi15050581
[10] Moslemi, Amin, Maria Rashidi, Ali Matin Nazar and Pejman Sharafi. "Advancements in vibration-based energy harvesting systems for bridges: A literature and systematic review." *Results in Engineering* (2025): 104622. https://doi.org/10.1016/j.rineng.2025.104622
[11] Yang, Xiaokang, Bo Niu, Kui He, Yahui Liu, Ruijie Xie and Bingke Xu. "Parameter effects on performance of piezoelectric wind energy harvesters based on the interaction between vortex-induced vibration and galloping." *Proceedings of the Institution of Mechanical Engineers, Part C: Journal of Mechanical Engineering Science* 238, no. 23 (2024): 11032-11048. https://doi.org/10.1177/09544062241272433
[12] Kawabata, Yusuke, Tsutomu Takahashi, Takeshi Haginoya and Masataka Shirakashi. "Interference effect of downstream strip-plate on the crossflow vibration of a square cylinder." *Journal of Fluid Science and Technology* 8, no. 3 (2013): 348-363. https://doi.org/10.1299/jfst.8.348
[13] Ismail, Mohamad Hafiz, Mohamed Sukri Mat Ali, S. A. Z. S. Salim, Masataka Shirakashi and Sallehuddin Muhamad. "Flow induced vibration of a square cylinder with high scruton number." *ratio* 1000, no. 2 (2006): 264.
[14] Methal, Zinnyrah, Mohamed Sukri Mat Ali, Nurshafinaz Mohd Maruai and Rasli Abd Ghani. "Microwatt energy harvesting by exploiting flow-induced vibration." *Journal of Advanced Research in Fluid Mechanics and Thermal Sciences* 47, no. 1 (2018): 25-34.
[15] Maruai, Nurshafinaz Mohd, Mohamed Sukri Mat Ali, Sheikh Ahmad Zaki, Jorge Alfredo Ardila-Rey and Izuan Amin Ishak. "The influence of different downstream plate length towards the flow-induced vibration on a square cylinder." *Scientific Reports* 13, no. 1 (2023): 17681. https://doi.org/10.1038/s41598-023-44388-w
[16] Mohamed, Azhar, Sheikh Ahmad Zaki, Masataka Shirakashi, Mohamed Sukri Mat Ali, Muhammad Zulfahmi Samsudin and Ahmad Faiz Mohammad. "Experimental Investigation of the Effect of a Downstream Square Plate on Vortex-induced Vibration and Galloping of a Square Cylinder." *Journal of Advanced Research in Fluid Mechanics and Thermal Sciences* 68, no. 1 (2020): 98-113. https://doi.org/10.37934/arfmts.68.1.98113
[17] Lucor, D., J. Foo and G. E. Karniadakis. "Vortex mode selection of a rigid cylinder subject to VIV at low mass-damping." *Journal of Fluids and Structures* 20, no. 4 (2005): 483-503. https://doi.org/10.1016/j.jfluidstructs.2005.02.002
[18] Zhang, Baoshou, Boyang Li, Song Fu, Wenjun Ding and Zhaoyong Mao. "Experimental investigation of the effect of high damping on the VIV energy converter near the free surface." *Energy* 244 (2022): 122677. https://doi.org/10.1016/j.energy.2021.122677
[19] Chasparis, Filippos, Yahya Modarres-Sadeghi, Franz S. Hover, Michael S. Triantafyllou, Michael Tognarelli and Pierre Beynet. "Lock-in, transient and chaotic response in riser VIV." In *International Conference on Offshore Mechanics and Arctic Engineering*, vol. 43451, pp. 479-485. 2009. https://doi.org/10.1115/OMAE2009-79444
[20] Kumar, Deepak, Amit Kumar Singh and Subhankar Sen. "Identification of response branches for oscillators with curved and straight contours executing VIV." *Ocean Engineering* 164 (2018): 616-627. https://doi.org/10.1016/j.oceaneng.2018.07.010
[21] Mannini, Claudio, A. M. Marra and Gianni Bartoli. "VIV–galloping instability of rectangular cylinders: Review and new experiments." *Journal of wind engineering and industrial aerodynamics* 132 (2014): 109-124. https://doi.org/10.1016/j.jweia.2014.06.021